Research Article

Amr Fouda*, Saad El-Din Hassan, Ahmed M. Eid, Mohamed A. Awad, Khalid Althumayri,
Naglaa Fathi Badr, and Mohammed F. Hamza

Endophytic bacterial strain, *Brevibacillus brevis*-mediated green synthesis of copper oxide nanoparticles, characterization, antifungal, *in vitro* cytotoxicity, and larvicidal activity

Abstract: The biomass filtrate containing various metabolites of endophytic bacterial strain, *Brevibacillus brevis* PI-5 was used as a biocatalyst for reducing and stabilizing copper oxide nanoparticles (CuO-NPs). UV-Vis spectroscopy, Fourier transform infrared, transmission electron microscopy, scanning electron microscopy with energy-dispersive X-ray (SEM-EDX), X-ray diffraction, and X-ray photoelectron spectroscopy were used for CuO-NPs characterization. A spherical, well-dispersed, and crystallographic structure with sizes of 2–28 nm was formed. The SEM-EDX confirmed the presence of Cu and O with weight percentages of 27.62% and 48.88%, respectively. The biological activities including antifungal, anticancer, and larvicidal of synthesized CuO-NPs were assessed using the fungal radial growth inhibition, MTT assay method, and mortality percentages, respectively. The obtained data showed that the CuO-NPs exhibit high activity in a dose-dependent manner. The growth of three phytopathogenic fungi, *Fusarium oxysporum, Alternaria alternata*, and *Aspergillus niger* was decreased by percentages of 64.5% ± 4.1%, 62.9% ± 0.3%, and 70.2% ± 2.3%, respectively at 300 μg·mL^{-1}. Also, various clinical *Candida* spp. were successfully inhibited with varied zones of inhibition and minimum inhibitory concentration values in ranges of 6.25–50 μg·mL^{-1}. The *in vitro* cytotoxicity exhibits target-orientation to breast cancer cells (T47D) at low concentration compared to normal cells (HFB4) with IC$_{50}$ values of 122.3 ± 5.4 and 229.9 ± 5.7 μg·mL^{-1}, respectively. The mortality percentages of I, II, III, and IV instar larvae of *Culex antennatus* were 60% ± 1.4%, 43.1% ± 1.1%, 36.2% ± 1%, and 32.1% ± 0.9%, at 10 mg·L^{-1} and increased to 86.9% ± 2.1%, 68.1% ± 1.7%, 64.4% ± 1.9%, and 53.1% ± 1.4% at 50 mg·L^{-1}, respectively.

1 Introduction

Nano-scaled materials are unique in many physical and chemical properties that distinguish them from their analogs of bulk materials. The application of these materials has been approved in the medical, environmental, and agricultural fields. Therefore, the science and technology of nanomaterials have gained increasing interest [1,2]. Recently, many highly stable nanoparticles have been produced by green synthesis, using environmentally friendly and efficient methods, making them safer alternatives to chemical and physical methods [3]. Wherefore, plants, algae, fungi, and bacteria were used to make non-toxic, low-cost, and energy-saving metallic-based nanoparticles [4]. Many thousands of these new materials are obtainable in the markets; moreover, they are integrated into various everyday products such as cosmetics, personal care, clothing, pharmaceutics, drug delivery, and food industry [5,6].

* **Corresponding author: Amr Fouda,** Department of Botany and Microbiology, Faculty of Science, Al-Azhar University, Nasr City, Cairo 11884, Egypt, e-mail: amr_fh83@azhar.edu.eg
Saad El-Din Hassan, Ahmed M. Eid: Department of Botany and Microbiology, Faculty of Science, Al-Azhar University, Nasr City, Cairo 11884, Egypt
Mohamed A. Awad: Department of Zoology and Entomology, Faculty of Science, Al-Azhar University, Nasr City, Cairo 11884, Egypt
Khalid Althumayri: Department of Chemistry, College of Science, Taibah University, 30002 Al-Madinah Al-Munawarah, Saudi Arabia
Naglaa Fathi Badr: Department of Zoology and Entomology, Faculty of Science (Girls brunch), Al-Azhar University, Nasr City, Cairo 11751, Egypt
Mohammed F. Hamza: School of Nuclear Science and Technology, University of South China, Hengyang 421001, China; Nuclear Materials Authority, POB 530, El-Maadi, Cairo 11728, Egypt

The bottom-up biogenic process is based on the biological reduction and oxidation by plant-extracted phytochemicals or microbial enzymes [7]. Moreover, bacteria offer fantastic benefits and potential for nanoparticle production as they are easy to culture, have a short generation period, facility for genetic modification, excellent stability, simple experimental conditions, and extracellular production of nanoparticles [8]. Therefore, metabolites of diverse bacterial strains such as *Bacillus cereus, Pseudomonas aeruginosa*, and *Shewanella oneidensis* were newly employed as reducing agents in the fabrication of Ag-NPs, ZnO-NPs, and Cu-NPs, respectively [9–11]. Many of these green synthesized nanoparticles showed a wide range of applications. For instance, Ag-NPs fabricated by leaf extract of *Trigonella foenum-graecum* exhibit antimicrobial activity against multi-drug resistant microbes, whereas those synthesized by leaf aqueous extract of *Moringa oleifera* displayed antifungal activity against *Puccinia striiformis* that causes stripe rust disease in wheat plant [12,13].

Among the metal oxide NPs, Cu-NPs/CuO-NPs have attracted attention due to their anticancer, antibacterial, antiviral, and antifungal properties and have been used in nanomedicine, as well as due to their beneficial effect on plants in terms of nutrition, growth, and defense [14]. Accordingly, CuO-NPs have been successfully induced from extracts of marine *Bacillus altitudinis*, and the executed cuprous oxide-NPs submitted great antibacterial attributes against the pathogenic strain *Pseudomonas aeruginosa* [15]. A low concentration of copper oxide nanoparticles (CuO-NPs) ($50 \mu g \cdot mL^{-1}$) derived from leaf extract of *Aerva javanica* plant manifested broad-spectrum activity against all the tested Gram-positive and Gram-negative bacteria, while $100 \mu g \cdot mL^{-1}$ of the biosynthesized CuO-NPs displayed enhanced antifungal potency against four *Candida* species. In the same regard, concentrations of CuO-NPs $>60 \mu g \cdot mL^{-1}$ showed significant toxicity on Neuro2A cells, and authors suggested that the CuO-NPs could be harmless when applied below this concentration [16]. Likewise, the myco-synthesized CuO-NPs and Ag-NPs considerably reduced the hyphal growth of the phyto-pathogenic fungi *Pyricularia oryzae* and *Alternaria alternata*, since CuO-NPs are less toxic than Ag-NPs, and they may be more useful in agricultural applications [17]. Recently, CuO-NPs were formed using a leaf aqueous extract of *Cissus vitiginea* with crystallite size of 32.32 nm and showed promising antioxidant activity [18]. Interestingly, Cu-NPs fabricated by extract of *Duranta erecta* leaf was used in water purification from organic dye contaminants [19]. In an interesting study about the toxicity of various concentrations of CuO-NPs and $CuSO_4 \cdot 0.5(H_2O)$ on the reproductivity and fertility of albino mice, the authors reported that the oral intake of CuO-NPs was safer to reproductive system of mice compared to the same concentration of $CuSO_4 \cdot 0.5(H_2O)$. Moreover the toxicological and histological changes appeared in the mice after treatment with $CuSO_4 \cdot 0.5(H_2O)$ [20]. These data indicate that the uses of CuO-NPs are safer than chemical compounds.

Considering the promising properties of nanomaterials as antibacterial and antifungal as well as anticancer properties, more efforts have been made to develop the properties of nano-metals and their oxides for mosquito control. Mosquitoes cause many diseases to be transmitted, resulting in millions of deaths annually, such as the parasite *Plasmodium* (which causes malaria), which infects 228 million cases worldwide annually, resulting in the death of 405,000 people in 2018 [21]. *Culex* mosquitoes are the main vector of the nematode (*Wuchereria bancrofti*) that causes filariasis which is one of the most dangerous and neglected diseases, whether in semi-urban or urban areas [22]. In the same context, the biotoxic impact of CuO-NPs/yttrium-doped CuO-NPs composite against *Culex pipiens* mosquito, recorded enhanced larvicidal activity with IC_{50s} values of 11.65 and $7.67 \, mg \cdot L^{-1}$, respectively [23]. Recently the biosynthesis of metal oxide nanoparticles using green approaches have increased, but the uses of endophytic bacterial strains for exploring their importance and their activities in bio-fabrication of small sizes and unique shapes of NPs are few. To the best of our knowledge, this is the first report for green synthesis of CuO-NPs using endophytic bacterial strain, *Brevibacillus brevis* isolated from medicinal plant, *Pulicaria incisa*. To this end, our study aimed for biosynthesis of CuO-NPs using the extracts of endophytic bacterial strain, *B. brevis* as a green, eco-friendly, rapid, cheap, and biocompatible method. The obtained cuprous oxide nanoparticles are characterized using UV-Vis spectroscopy, Fourier transform infrared (FTIR), transmission electron microscopy (TEM), scanning electron microscopy with energy-dispersive X-ray (SEM-EDX), X-ray diffraction (XRD), and X-ray photoelectron spectroscopy (XPS). The potential of bio-synthesized CuO-NPs in *in vitro* cytotoxicity against cancer and normal cell lines, antifungal activity against phyto-pathogenic fungi and various clinical *Candida* species, and larvicidal activity against I, II, III, and IV instar larvae of *Culex antennatus* were investigated.

2 Materials and methods

2.1 Bacterial strain

The CuO-NPs were synthesized using an endophytic bacterial strain, *Brevibacillus brevis* PI-5. This strain was

isolated previously from leaves of the medicinal plant, *Pulicaria incisa* collected from Saint Katherine, South Sinai, Egypt [24]. The isolation procedure was achieved by washing the collected healthy plant leaves with tap water to remove any debris that adhered to the collected samples. After that, the collected plant leaves were subjected to surface sterilization by soaking in sterile distilled water for 1 min, followed by soaking in ethanol (70% v/v) for 1 min, sodium hypochlorite (2.5%) for 4 min, ethanol (70% v/v) for 30 s, and finally washed thrice with sterilized distilled water. The surface sterilization of plant samples was confirmed by the absence of growth of bacteria, fungi, and actinomycetes on appropriate growth media inoculated by the last washing in distilled water [25]. The endophytic bacterial strains were isolated by cutting the sterilized samples to small parts (6 mm) and put approximately four parts on the surface of nutrient agar plate containing nystatin ($25\,\mu\text{g·mL}^{-1}$) to inhibit the growth of fungal species. The loaded plates were incubated for 48 h at 35°C and observed daily to pick-up any bacterial colony growth around plant parts and re-inoculated onto the new plate.

The endophytic bacterial strain used in the current study was identified based on morphological, physiological, and biochemical tests [26], and confirmed the identification by amplification and sequencing of the 16 S rRNA gene. The obtained sequence was deposited in GenBank under the accession number MT994671.

2.2 Bacterial synthesis of CuO-NPs

The endophytic bacterial strain, PI-5 was inoculated in 500 mL nutrient broth media and incubated at 35°C ± 2°C for 24 h under shaking conditions (150 rpm). At the end of the incubation period, the inoculated nutrient broth media was centrifuged at 5,000 rpm for 15 min to collect bacterial biomass which was rinsed thrice with distilled H_2O to remove media components adhering. After that the collected bacterial biomass was suspended in distilled H_2O ($0.1\,\text{g·mL}^{-1}$) for 24 h in dark conditions, followed by centrifugation to collect the supernatant (bacterial biomass filtrate) which was used as a biocatalyst for reducing metal precursor ($Cu(CH_3COO)_2·H_2O$, Sigma Aldrich) to form CuO-NPs as follows: 100 µg metal precursor was dissolved in 3 mL of distilled H_2O and added to 97 mL of collected bacterial biomass filtrate to get a final concentration of 5 mM. The previous mixture was stirred at 100 rpm for 1 h and adjusted the pH of the solution to 8 by using 1 N NaOH that was added drop-wise [27]. The as-formed greenish precipitate was collected by centrifugation at 5,000 rpm for

15 min, washed twice with distilled H_2O, and oven-dried at 100°C for 24 h.

2.3 Characterization of bacterial-synthesized CuO-NPs

2.3.1 UV-Vis spectroscopy

The color change of bacterial biomass filtrate after being mixed with $Cu(CH_3COO)_2·H_2O$ as a sign of successful formation of CuO-NPs was monitored by UV-Vis spectroscopy (JENWAY 6305, Staffordshire, UK). In this method, 2 mL of synthesized CuO-NPs solution was put in a cuvette and the color absorbance was measured at a wavelength of 200–800 nm, at regular intervals.

2.3.2 FTIR spectroscopy

The functional groups involved in bacterial biomass filtrate and their role in the fabrication of CuO-NPs were detected by FTIR (Agilent system Cary 660 FTIR model) using the potassium bromide (KBr) method. In this analysis, 10 mg CuO-NPs powder was mixed with KBr, pressed well to form a disk, and scanned in the ranges of 400–4,000 cm^{-1} [28].

2.3.3 TEM

The morphological characteristics (size and shape) of bacterial-synthesized CuO-NPs were investigated by TEM (JEOL 1010, Japan, 200 kV, X25000). For this analysis, the carbon grid was loaded with a few drops of diluted CuO-NPs solution and subjected to vacuum desiccation overnight to dry before being analyzed [29].

2.3.4 SEM-EDX

The chemical composition (qualitative and quantitative) of the bacterial-synthesized CuO-NPs was investigated by EDX (JEOL, JSM-6360LA, Japan) through SEM analysis [30].

2.3.5 XRD

The nature (crystalline or amorphous) of synthesized CuO-NPs was investigated using XRD (X'Pert PRO, Philips,

Eindhoven, Netherlands) at a 2θ scale of 10–80°. The scanning was achieved at a condition of 40 kV (voltage); 30 mA (current); and the X-ray radiation source was Cu Kα. By XRD analysis, the average crystallite size was measured by Scherrer's equation [31]:

$$D = \frac{0.89 \times 1.54}{\beta \cos\theta} \quad (1)$$

where D is the average crystal size of CuO-NPs, 0.89 is the Scherrer's constant, 1.54 is the *X*-ray wavelength, β is half of the maximum intensity, and θ is the Bragg's diffraction angle.

2.3.6 XPS

The quantitative elemental composition of the surface of synthesized CuO-NPs was investigated by XPS. This analysis was performed using ESCALAB 250 XI$^+$ (Thermo Fischer Scientific Inc., Waltham, MA, USA) connected with a source of radiation, monochromatic X-ray Al-Kα (1,486.6 eV). The analysis conditions were 10^{-8} mbar for the prepared CuO-NPs sample, the energy was adjusted using Ag 3d$_{5/2}$ signal (ΔBE: 0.45 eV), C 1s signal (ΔBE: 0.82 eV), size spot was adjusted at 500 µm, the energies of the narrow and full-spectrum pass were 20 and 50 eV, respectively [32].

2.4 Antifungal activity

2.4.1 Activity of CuO-NPs against phytopathogenic fungi

The activity of bacterial-synthesized CuO-NPs was investigated against some phytopathogenic fungi including *Fusarium oxysporum*, *Alternaria alternata*, and *Aspergillus niger* collected from the Department of Plant Pathology, Faculty of Agriculture, Zagazig University. In this method, an agar plug (8 mm) of each fungal strain covered with heavy growing mycelia was inoculated in the center of potato dextrose agar (PDA) media supplemented with 200 µL of CuO-NPs that were prepared at different concentrations (300, 200, and 100 µg·mL^{-1}). After that, the inoculated plates were incubated at 28°C ± 2°C for 5 days. At the end of the incubation period, the fungal radial growth was measured, and the growth inhibition was calculated according to the following equation [17]:

where radial growth of control is the diameter of fungal growth after 5 days under the same incubation conditions in the absence of CuO-NPs.

2.4.2 Activity of CuO-NPs against different clinical pathogens *Candida* spp.

The anti-*Candida* activity of CuO-NPs was evaluated by agar well diffusion method against four clinical species designated as *C. albicans*, *C. glabrata*, *C. tropicalis*, and *C. parapsilosis*. These strains were obtained and identified using traditional and molecular methods in Microbiology Laboratory, National Research Center, Cairo, Egypt. In this method, 50 µL of fresh *Candida* sp. (optical density (OD) = 1) was inoculated in 100 mL of yeast extract peptone dextrose agar media, shaking well, and poured under aseptic conditions into Petri dishes. Upon media solidification, four well (7 mm) were prepared in each plate and filled with 100 µL of prepared CuO-NPs solution (200 µg·mL^{-1}). The loaded plates were kept in the refrigerator for 1 h before being incubated at 30°C ± 2°C for 24 h. At the end of the incubation period, the results were recorded as the diameter of the inhibition zone (mm) formed around each well. DMSO (solvent system) was used as a negative control. The same experiment was repeated with different CuO-NPs concentrations (100, 50, 25, 12.5, 6.25, and 3.125 µg·mL^{-1}) to detect the minimum inhibitory concentration (MIC) based on the lowest concentration that inhibits the *Candida* growth [33]. The experiment was carried out in triplicates.

2.5 *In vitro* cytotoxicity assay

2.5.1 Cell lines culture

The T47D (epithelial cells, ductal carcinoma, breast tissue, mammary gland) and HFB4 (adherent cells, normal melanocytes) cell lines were purchased from the Holding Company for Biological Products and Vaccines (VACSERA) Cairo, Egypt.

2.5.2 MTT assay

The *in vitro* cytotoxic efficacy of CuO-NPs fabricated by endophytic bacterial strain against T47D and HFB4 cell

$$\text{Growth inhibition percentages(\%)} = \frac{\text{Radial growth of control} - \text{Radial growth of treated sample}}{\text{Radial growth of control}} \times 100 \quad (2)$$

lines was evaluated by conducting a dimethyl thiazolyl tetrazolium bromide (MTT) assay. The two tested cells were grown in 96-well tissue culture plates (100 μL/well, 1×10^5 cells) and incubated at 37°C in a humidified condition, 5% CO_2 incubator for 24 h. After forming a confluent sheet, the cell monolayer was washed twice with washing media and incubated for 48 h in maintenance media (RPMI medium with 2% serum) treated with various concentrations (1,000, 500, 250, 125, 62.5, and 31.25 μg·mL^{-1}) of synthesized CuO-NPs, 3 wells receiving only media without CuO-NPs as a control. After incubation, culture media were decanted and 50 μL of fresh MTT solution (5 mg·mL^{-1} in PBS, Bio Basic Canada Inc.) were added to each well, thoroughly mixed for 5 min on a shaking condition (150 rpm), and plates were incubated for 4 h to allow metabolization of MTT. After incubation, media were dumped off and the developed formazan crystals were dissolved in DMSO (10%) and plates were shacked in dark for 30 min. Finally, the OD of the formed color was measured at 570 nm in a multi-well ELISA plate reader [34]. Changes in cell morphology were visualized by a phase-contrast microscope, and cell viability was calculated by the following equation:

$$\text{Cell viability}(\%) = \frac{\text{Absorbance of treated sample}}{\text{Absorbance of control}} \times 100$$

(3)

2.6 Mosquitocidal activity

2.6.1 Mosquito rearing

The larvae of *Culex antennatus* mosquito species were obtained from the Entomology Laboratory, Faculty of Science, Al-Azhar University, Cairo, Egypt. The collected larvae were put in a plastic container covered with tap water and kept under *in vitro* conditions. The experiment was achieved under relative humidity percentages of 70–80%, a temperature of 27°C ± 2°C, and a photoperiod of 12:12 light/dark. The dog biscuits mixed with yeast were used for larvae feeding under laboratory conditions.

2.6.2 Bioassay

The efficacy of bacterial-synthesized CuO-NPs against I, II, III, and IV instar larvae of *C. antennatus* was done according to standard methods of WHO [35] with slight modification. Approximately, 25 *C. antennatus* larvae from each instar were transferred to the cup containing 100 mL of CuO-NPs at different concentrations (10, 20, 30, 40, and 50 mg·L^{-1}), whereas the cup containing 100 mL of dechlorinated tap water was used as a control. The experiment was conducted in five replicates for each CuO-NPs concentration. The larvae were considered dead when they lost their ability to reach the treatment solution surface after disturbing the cups. The mortality percentages were calculated after 48 h using the following equation [36]:

$$\text{Mortality percentages (\%)} = \frac{\text{Mortality in treatment} - \text{Mortality in control}}{100 - \text{Mortality in control}} \times 100$$

(4)

2.7 Statistical analysis

Data obtained in the current study are represented as the mean values of three independent replicates. Data were analyzed using the statistical package SPSS v17. The mean difference comparison between the treatments was analyzed by the *t*-test or the analysis of variance (ANOVA) and subsequently by the Tukey HSD test at $p < 0.05$. The larvae mortality percentages were analyzed using probit analysis, with LC$_{50}$ and LC$_{90}$ calculated using Finney's method.

3 Result and discussion

3.1 Endophytic bacterial strain mediated green synthesis of CuO-NPs

Green synthesis of nanomaterials is becoming more popular, safe, and cost-effective. Among green synthesis, endophytic microorganisms such as bacteria, actinomycetes, and fungi have the high potential to convert metal and metal oxide ions to nanoscale structures [37]. Amongst endophytic microbes, bacterial strains possess the potential to establish various defense mechanisms to ameliorate the toxicity of accumulated metal ions inside the plant cells by converting them to the nanoscale, therefore it is a candidate to become a good producer of nanoparticles [38]. In addition, the huge metabolites produced by endophytic bacteria are used to reduce metal-to-metal nanoparticles and enhance the stability of fabricated nanostructure [39]. In the current study, the metabolites secreted by the endophytic bacterial strain, *Brevibacillus brevis* PI-5 were harnessed to fabricate CuO-NPs. These metabolites were used as a reducing agent for Cu(CH$_3$COO)$_2$·H$_2$O to form CuO-NPs followed by capping of the final product to enhance their stability. Change in biomass filtrate color after mixing with metal precursor is an incredibly useful indicator for
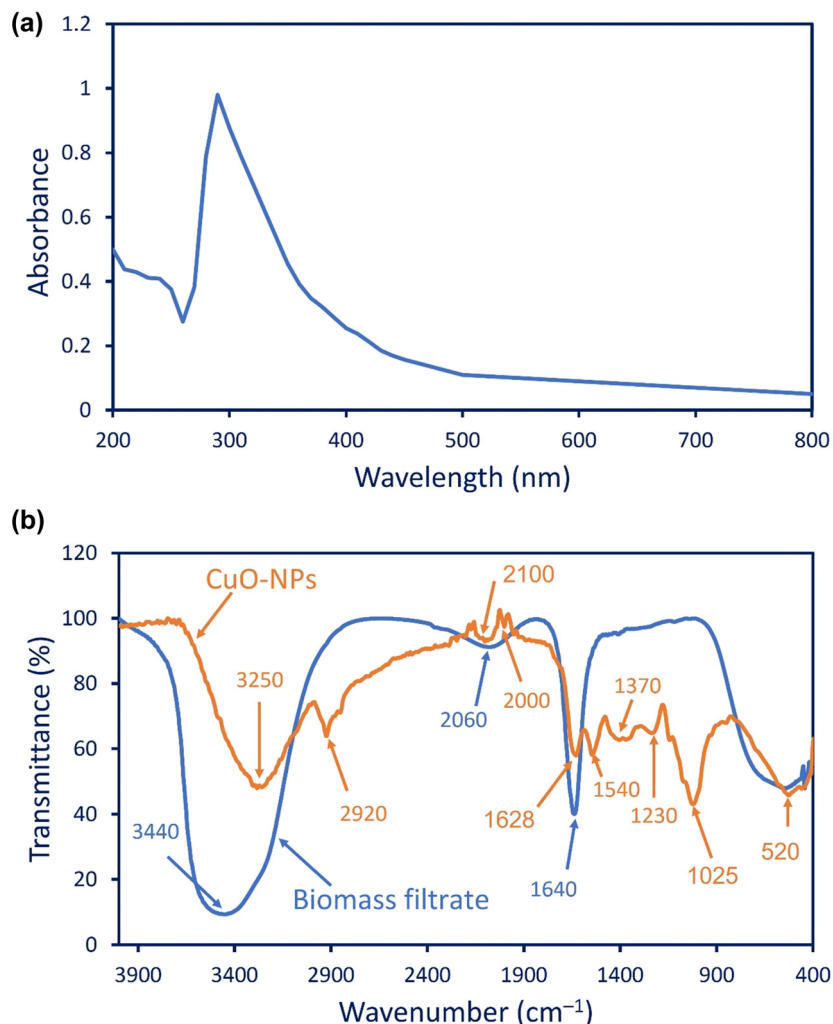
Figure 1: (a) UV-Vis spectroscopy showed the maximum SPR of bacterial-synthesized CuO-NPs at 290 nm and (b) FTIR of endophytic bacterial biomass filtrate and fabricated CuO-NPs showed various functional groups.

successful NPs fabrication [40]. Herein the first monitor for the successful formation of CuO-NPs by endophytic bacterial strain EP-1 was the change in biomass filtrate from colorless to greenish color. In contrast, no color change in bacterial biomass filtrate was incubated under the same condition in the absence of metal precursor. The change in color is attributed to charged particle vibration existing on the NPs surface and resonance [31]. The obtained data agree with those reported that the biomass filtrate of *Pseudomonas fluorescens* was changed from blue (original color) to greenish after mixing with $CuSO_4$ solution indicating the formation of CuO-NPs [41]. Similarly, the biomass filtrate of endophytic actinomycetes, *Streptomyces zaomyceticus*, and *Streptomyces pseudogriseolus* was changed from pale blue to greenish color after mixing with $Cu(CH_3COO)_2 \cdot H_2O$ [42].

3.2 Characterization of CuO-NPs

3.2.1 UV-Vis spectroscopy

The greenish color intensity that formed due to the mixing of biomass filtrate of endophytic bacteria strain with $Cu(CH_3COO)_2 \cdot H_2O$ was investigated using UV-Vis spectroscopy at a varied wavelength of 200–800 nm (Figure 1a). Data showed that the maximum absorption peak was observed at 290 nm which correlated to the maximum surface plasmon of CuO. The obtained data are compatible with the absorption peak of CuO-NPs in the published literature [29]. The UV-Vis analysis is more sensitive to size, shape, concentration, and refractive indices near the NPs surface because of the unique optical NPs properties [31]. Therefore, UV-Vis spectroscopy is considered a

useful technique for the identification and characterization of NPs. In the current study, the appearance of a single peak in the UV chart predicted that the shape of green synthesized CuO-NPs is spherical as reported previously [43].

3.2.2 FTIR spectroscopy

The functional groups related to various compounds present in bacterial biomass filtrate and their role in reducing, capping, and stabilizing CuO-NPs were detected using FTIR (Figure 1b). As shown, the bacterial biomass filtrate has three absorption peaks at 1,640, 2,060, and 3,440 cm^{-1}. The strong observed peak at 1,640 cm^{-1} can be signifying to (the amide I and II of proteins) and (stretching C=O of polysaccharide moieties) secreted by bacterial strain [9]. The peak at 2,060 cm^{-1} is attributed to the stretching CO of unsaturated ester and carboxylic compounds, whereas the peak at 3,440 cm^{-1} can be related to the stretching O–H of hydroxyl groups that overlapped with stretching N–H of aliphatic primary amines [44,45]. The IR spectra of CuO-NPs showed varied intense peaks at different wavelength values (Figure 1b). The strong broad peak at 3,250 cm^{-1} is attributed to the stretching O–H of carboxylic acid, whereas the medium peak at 2,920 cm^{-1} corresponds to the stretching C–H of alkane [46]. The medium observed peak in 2,000 cm^{-1} is signified by stretching C=C=C of allene, while the peak at 2,100 cm^{-1} is related to C≡C stretch of alkyne [47]. Peaks at 1,628 and 1,540 cm^{-1} are corresponding to either C=N (carbonyl groups), C=O (carboxylic group), or C=C (primary and secondary amides) [48,49]. The medium peaks at 1,370 and 1,230 cm^{-1} are corresponding to stretching S=O and C–N of sulfonamide and amine, respectively, whereas the strong peak at 1,025 cm^{-1} can be related to the deformation of stretching CO or OH of alcoholic and phenolic groups, respectively [50]. The presence of CuO in the sample was confirmed at a wavenumber of 520 cm^{-1}. The obtained data are completely in agreement with various studies that confirmed that the peak of CuO-NPs was in the range of 400–700 cm^{-1} [51–53]. The presence of various functional groups such as an alkane, alkyne, amines, phenolic, carbonyl, and carboxylic groups was important for the reduction of metal precursors to form metal oxide nanoparticles (CuO-NPs) followed by capping and stabilizing the final product.

3.2.3 TEM

The size, surface charge, shape, biocompatibility, agglomeration, and stability of NPs are considered the main parameters that influenced their biological and biotechnological activities [7]. TEM analysis is a useful method for the determination of sizes, shapes, and agglomeration of synthesized NPs. As seen, the CuO-NPs fabricated by endophytic bacterial strain, *B. brevis* PI-5 were spherical in shape, well-dispersed with sizes of 2–28 nm, and average particle size of 10.8 ± 4.5 nm (Figure 2a and b). The obtained result was compatible with those reported that the average size of CuO-NPs synthesized by aqueous extract of pumpkin seeds was 20 nm [54]. Also, the TEM analysis of CuO-NPs fabricated by *Streptomyces* sp. strain MHM38 revealed that the average size was in the range of 1.7–13.5 nm [55]. The activity of CuO-NPs was size- and shape-dependent as previously reported. For instance, the antibacterial activity of CuO-NPs against *E. coli*, *P. aeruginosa*, *B. subtilis*, and *S. aureus* was dependent on size. The highest antibacterial activity was recorded for the size of 20 nm followed by 21, 25, and 27 nm, respectively [56]. Mancuso and Cao reported that the CuO-NPs at the nanoscale in the range of 20–50 nm were more toxic as compared with micro-size particles [57]. Moreover, the removal of methyl orange dye using NPs was more effective for spherical shapes followed by hexagonal, cuboidal, and cylindrical shapes [58]. The activity of zinc oxide nanoparticles with nano-rod shape against various pathogenic microbial strains and cancerous cell lines was more effective compared to hexagonal shape [59]. Due to the smaller size of the bacterial-synthesized CuO-NPs in the current study, we can predict their high biological activity.

3.2.4 SEM-EDX

The EDX microanalysis is a useful technique used to detect the qualitative and quantitative elements in the prepared sample based on the emission of specific X-rays [60]. In the current study, the elementary mapping of the bacterial-synthesized CuO-NPs was analyzed using EDX (Figure 2c). As shown, one peak for O was shown at 0.5 keV, and three peaks for Cu were observed at 1, 8, and 9 keV indicating the successful formation of CuO-NPs as reported previously [61]. The elementary mapping revealed that the prepared sample contains C, O, and Cu with weight percentages of 23.5%, 27.62%, and 48.88% and atomic percentages of 35.71%, 49.44%, and 14.85%, respectively. The presence of C can be attributed to the scattering of capping agents such as carbohydrates, proteins, and polysaccharides due to X-ray emission [55,62]. No other additional peaks in the EDX chart imply that the synthesized CuO-NPs were highly pure. Similarly, the EDX chart of CuO-NPs synthesized by endophytic actinomycetes

(a)

(b)

(c)

Element	Weight (%)	Atomic (%)
C K	23.5	35.71
O K	27.62	49.44
Cu K	48.88	14.85
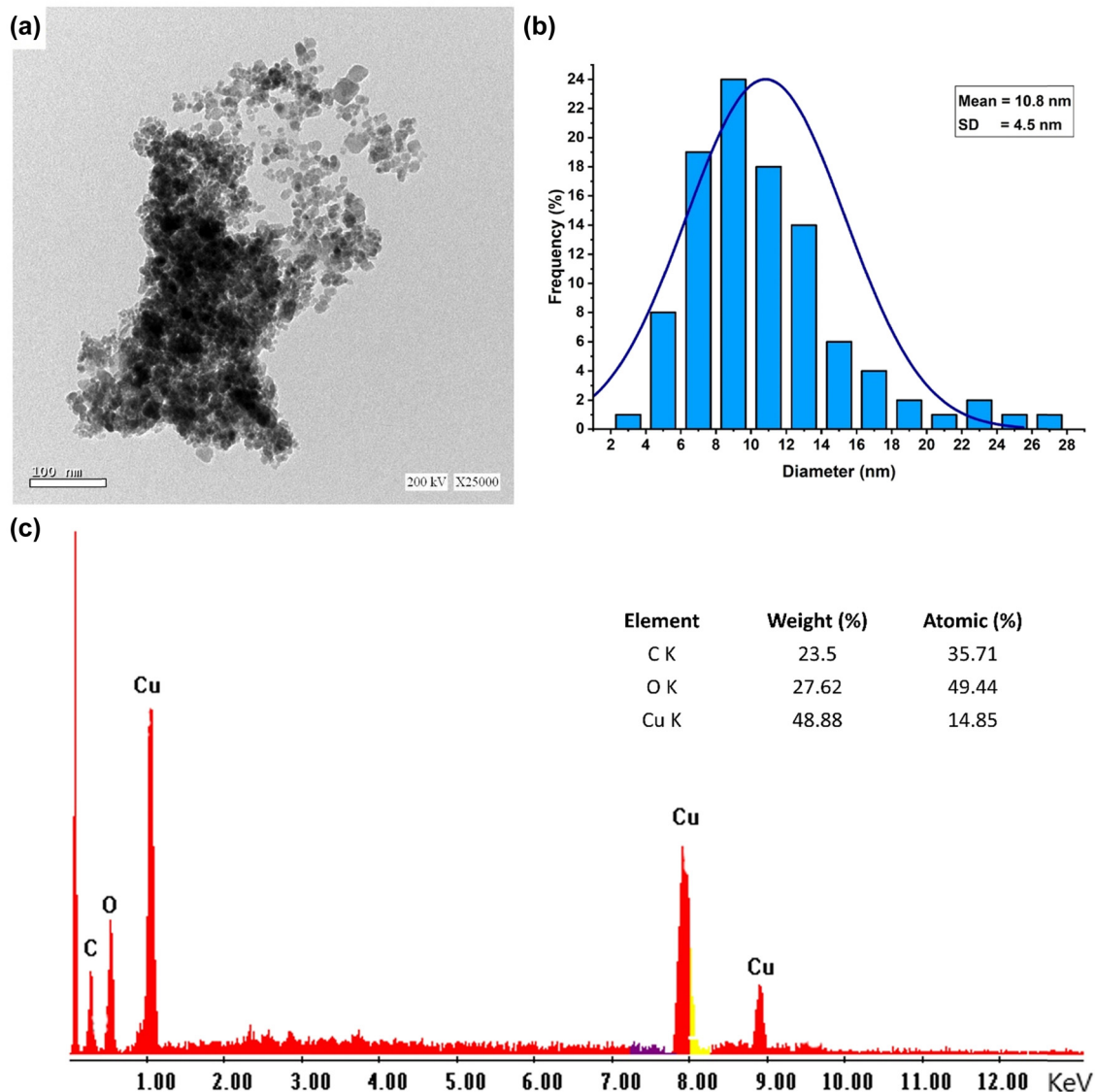
Figure 2: Characterization of CuO-NPs synthesized by endophytic bacterial strain, *B. brevis*. (a) TEM analysis showed spherical shape, (b) size distribution of synthesized CuO-NPs showed average particle size of 10.8 ± 4.5 nm, and (c) EDX chart showing the sample containing Cu, O, and C.

contains Cu and O with weight percentages of 75.5% and 24.5% and atomic percentages of 57.8% and 42.2%, respectively [29].

3.2.5 XRD

The XRD analysis was achieved to examine the purity and crystalline phase of as-formed nanoparticles. Figure 3 showed the XRD pattern of bacterial-synthesized CuO-NPs and exhibit the presence of 8 diffraction peaks at 2θ degrees of 32.62°, 35.6°, 38.68°, 48.8°, 53.68°, 58.4°, 61.58°, and 66.48° which corresponds to plane peaks of (110), (002),

(111), (−202), (020), (202), (−113), and (310), respectively. The obtained data affirm the synthesized monoclinic crystalline CuO-NPs according to JCPDS (80-1916) [16]. The obtained results are compatible with previous studies on the green synthesis of CuO-NPs [47,63]. According to the XRD pattern, the presence of well-defined and sharp diffraction peaks confirmed the crystallinity nature of synthesized CuO-NPs with a size less than 100 nm [64]. Naz et al. reported that the presence of diffraction peak in XRD pattern in 2θ range of 35–39° confirmed the successful formation of CuO-NPs [65]. The absence of additional diffraction peaks in the XRD pattern indicates that the purity of synthesized CuO-NPs is high and this
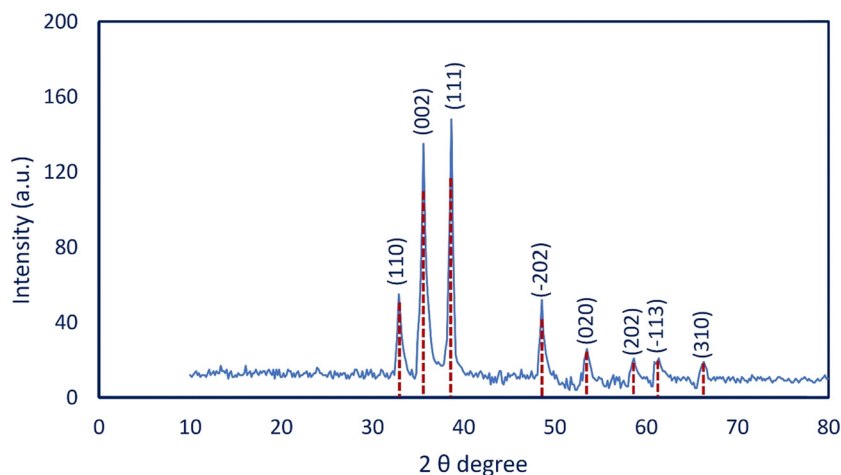
Figure 3: XRD pattern of CuO-NPs synthesized by endophytic bacterial strain *B. brevis*.

finding was compatible with EDX analysis. The crystallite size of CuO-NPs can be calculated based on XRD analysis using Scherrer's equation which was 19 nm. A similar result was observed by Amin et al. who reported that the crystallite size of CuO-NPs fabricated by leaf aqueous extract of *Aerva javanica* was 15 nm based on a calculation using Scherrer's equation [16].

3.2.6 XPS

Figure 4a shows the XPS survey spectra of the CuO-NPs. It confirms the presence of the Cu element by different formations (binding energy), i.e., (Cu 3p3, Cu 2p1, Cu 2p3, Cu 2s, Cu LM1, and Cu LM2). In addition, other elements either reflect the structure (C 1s, N 1s, O 1s, and O KL1, O KL2) or are related to the metabolites (Na 1s and Na 2s). The C 1s (Figure 4b) was split into six internal peaks corresponding to the hydrocarbon skeletal, i.e., C=C, C(H, C), C(S, N), C–OH, C–O–C, and O–C=O, these peaks have appeared at 283.95, 284.83, 285.75, 286.6, 288.3, and 289.15 eV, respectively [28,66]. The O 1s (Figure 4c) was deconvoluting to four peaks confirming both hydrocarbons and impeded CuO with Na element; these peaks appeared at 529.75, 531.21, 532.35, and 535.9 for O–Na, O (Cu(II), C,H), O–C=O, and C–O–C, NaKLL [32,67], respectively. These peaks are parallel to the FTIR analysis which shows NH, C=O, and C–O. N 1s (Figure 4d) was split into two peaks for N(C, H) at a bending energy of 400.04 eV [68]. The Cu(II) (Figure 4e) shows mainly Cu 20 3/2 peaks verifying the Cu(II) species. This peak was split into two peaks at 932.87 and 934.45 eV. From these data (especially from O 1s and Cu 2p), it can concluded that the Cu was found in the sample as divalent oxide.

3.3 Antifungal activity

Fungi are considered one of the main pathogens for plants, animals, and humans. The world's crops are subjected to annual loss of 10–15% due to plant disease, and 70–80% of these diseases are caused by fungi [69]. Therefore, the discovery of new active compounds to cope with these losses is considered one of the main challenges. In the current study, the activity of different concentrations of CuO-NPs synthesized by endophytic bacterial strain as a green approach was assessed to inhibit the growth of three important phytopathogens, *Fusarium oxysporum*, *Alternaria alternata*, and *Aspergillus niger*. Data analysis revealed that the inhibitory effects of CuO-NPs were dependent on the concentration and the type of fungi. At low concentration (100 µg·mL^{-1}), the inhibition percentages of *A. niger*, *F. oxysporum*, and *A. alternata* were 47.1% ± 3.3%, 43.4% ± 2.9%, and 41.7% ± 2.5%, respectively (Figure 5). The inhibitory percentages were increased with the increase in the CuO-NPs concentrations to 58.5% ± 2.4%, 52.8% ± 3.3%, and 50.9% ± 1.9% for a concentration of 200 µg·mL^{-1} and 70.2% ± 2.3%, 64.5% ± 4.1%, and 62.9% ± 0.3% for a concentration of 300 µg·mL^{-1} against *A. niger*, *F. oxysporum*, and *A. alternata*, respectively (Figure 5). As shown, *A. niger* was highly sensitive to bacterial-synthesized CuO-NPs followed by *F. oxysporum*, and *A. alternata*. In a recent study, the CuO-NPs synthesized by endophytic *Streptomyces* spp. were more active against phytopathogen *A. niger* with a maximum inhibition percentage of 75% followed by *A. alternata*, *F. oxysporum*, and *Pythium ultimum* with varied inhibition percentages [42]. Various metal-NPs, metal oxide-NPs, and nanocomposites such as Ag-NPs, Cu-NPs, ZnO-NPs, and CuO/C
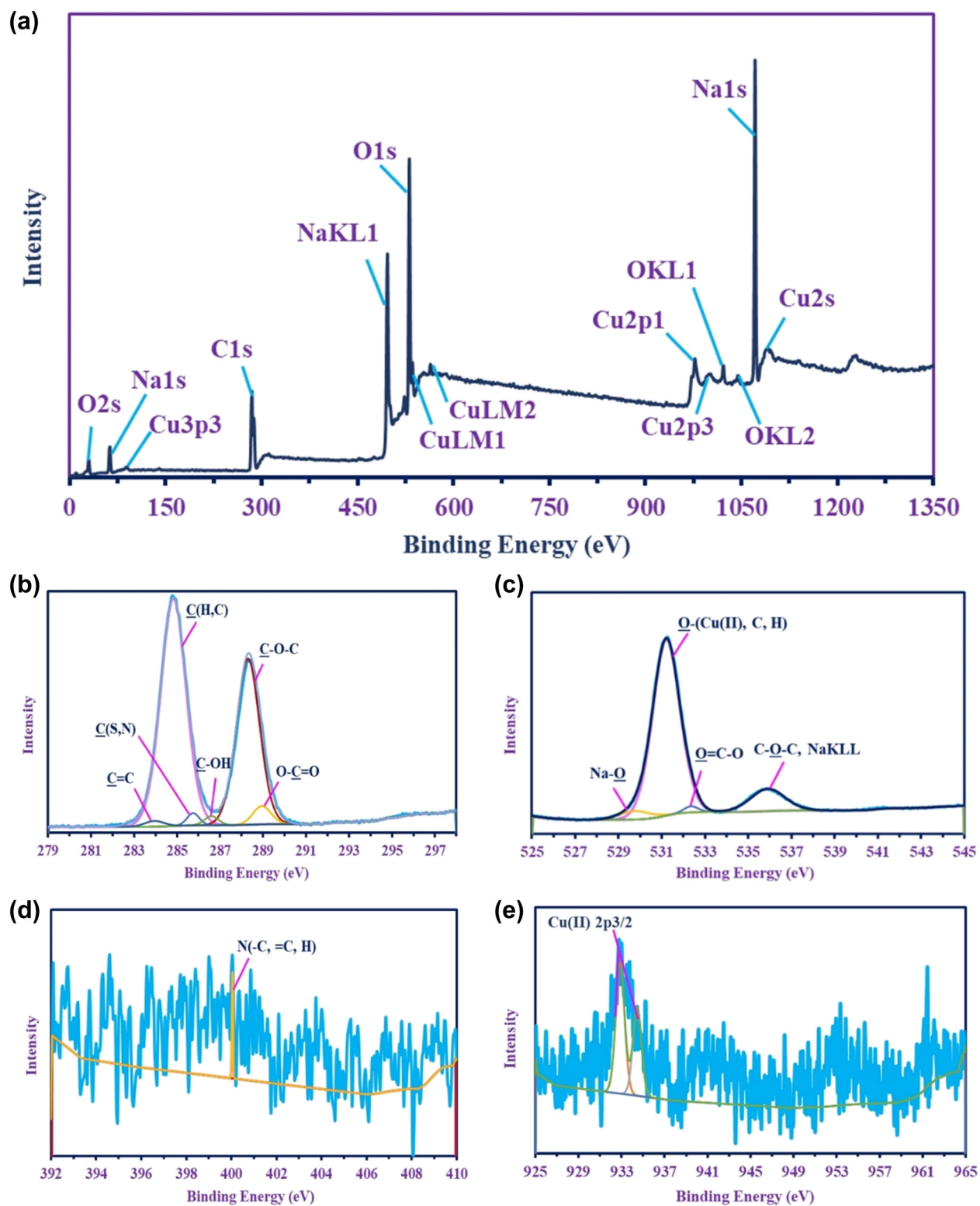
Figure 4: The XPS analysis of CuO-NPs synthesized by endophytic bacterial strain *B. brevis*. (a) XPS survey, (b−e) C 1s, O 1s, N 1s, and Cu2p, respectively.
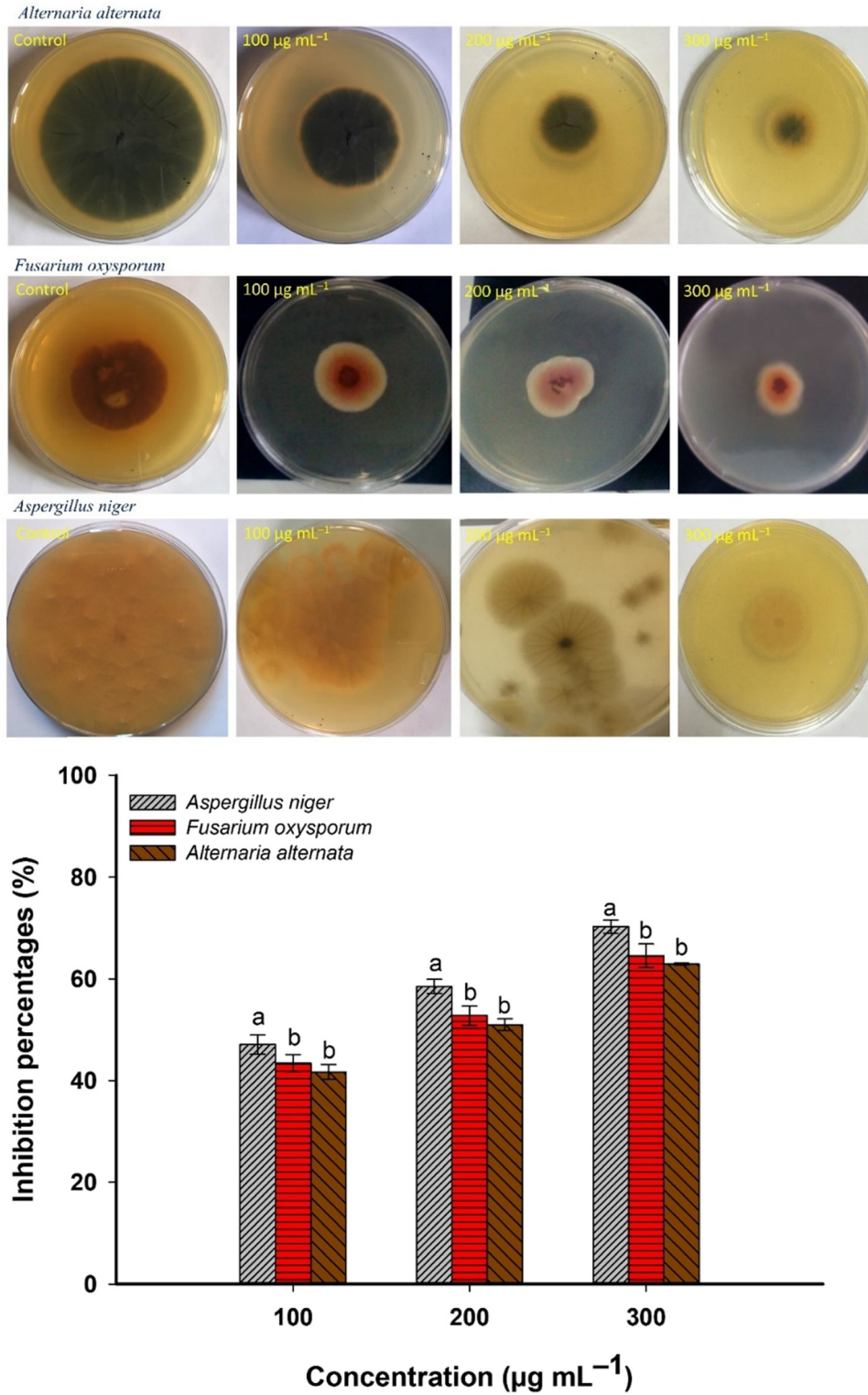
Figure 5: The mycelial growth inhibitions of three phytopathogens, *F. oxysporum*, *A. alternata*, and *A. niger* growing on potato dextrose agar media supplemented with different concentrations (300, 200, and 100 µg·mL⁻¹) and incubation for 5 days.

especially those fabricated by green methods are utilized as a safe agent to control different phytopathogenic fungi [70–72].

Diseases caused by *Candida* spp. have increased especially in the last decade and are responsible for nosocomial infections that cause serious health issues

worldwide [73]. Therefore, it is urgent to discover new active compounds to overcome the health problems caused by *Candida* spp. In the current study, the activity of CuO-NPs against various clinical *Candida* isolates, *C. albicans, C. glabrata, C. tropicalis*, and *C. parapsilosis* was investigated using the agar well diffusion method. Analysis of variance revealed that the activity of bacterial-synthesized CuO-NPs was dose-dependent. The obtained data are compatible with those reported that the anti-*Candida* activity of CuO/C nanocomposite synthesized by leaf aqueous extract of *Adhatoda vasica* was concentration-dependent [72]. The negative control which was DMSO as a solvent system does not exhibit activity against any *Candida* species. The highest inhibition zones were 19.3 ± 0.7, 16.7 ± 1.5, 19 ± 1, and 13.7 ± 0.7 mm for *C. albicans*, *C. glabrata*, *C. tropicalis*, and *C. parapsilosis*, respectively at a maximum CuO-NPs concentration (200 μg·mL^{-1}) (Figure 6). The diameter of inhibition zones was reduced by decreasing the concentrations of CuO-NPs. For instance, at a concentration of 100 μg·mL^{-1}, the diameter of the zone of inhibition was 16.7 ± 0.7, 15.3 ± 0.6, 17.3 ± 0.6, and 12.3 ± 0.5 mm for *C. albicans*, *C. glabrata*, *C. tropicalis*, and *C. parapsilosis*, respectively. Whereas these inhibition zones were reduced to 15.3 ± 0.6, 15 ± 1, 15.7 ± 1.2, and 10 ± 1 mm at a concentration of 50 μg·mL^{-1} for the same previous sequence of *candida* species (Figure 6). In harmony with the obtained data, the highest inhibition zones of 34.2 ± 1.4 and 23.7 ± 1.5 mm were attained due to treatment of *C. albicans* and *C. glabrata* with 100 μg·mL^{-1} of CuO-NPs fabricated by leaf aqueous extract of *Achillea millefolium* [74]. These zones of inhibitions were reduced to 19.5 ± 0.6 and 18.6 ± 1.2 mm, and
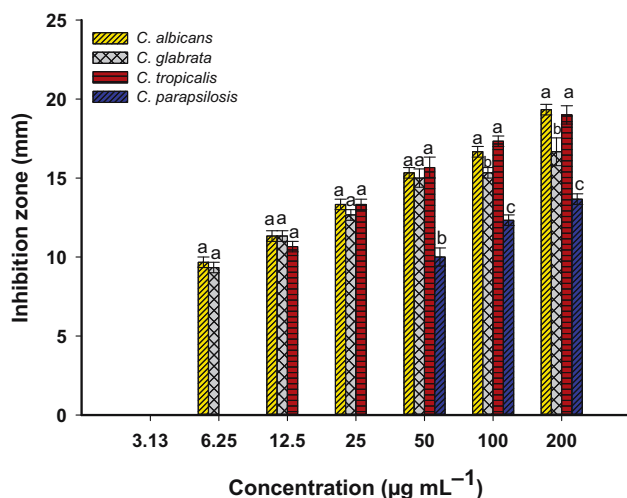
11.6 ± 0.5 and 15.2 ± 1.4 mm at 50 and 10 μg·mL^{-1} of CuO-NPs, respectively. Also, CuO-NPs synthesized by harnessing metabolites secreted by *Aerva javanica* showed anti-*Candida* activity against *C. albicans*, *C. tropicalis*, and *C. krusei* with zones of inhibitions of 9 + 0.5, 4 ± 0.0, and 5 ± 1 mm at a concentration of 100 μg·mL^{-1} [16]. The CuO-NPs fabricated by different bacterial species, namely, *Rhodococcus*, *Marinomonas*, *Brevundimonas*, *Pseudomonas*, and *Bacillus* isolated from Antarctic ciliate *Euplotes focardii* showed high anti-*Candida* activity against *C. albicans* and *C. parapsilosis* with clear zones in the range from 16 ± 0.4 mm to 18 ± 0.4 mm as compared with clear zone formed by CuSO$_4$ (11 ± 0.2 mm) [75]. Moreover, Ag-NPs fabricated by aqueous extract of *Alhagi graecorum* displayed high activity against various *Candida* strains designated as *C. glabrata*, *C. albicans*, *C. tropicales*, *C. parapsilosis*, and *C. krusei* with inhibition zones in the range of 14–27 mm according to concentration used [76].

Successful infection control depends on the strategy of treatment that is selected according to the dependable evaluation of MIC [77]. Our study revealed that the lowest MIC value of 6.25 μg·mL^{-1} was assigned against *C. albicans* and *C. glabrata* with inhibition zones of 9.7 ± 0.6 and 9.3 ± 0.6 mm, respectively. The MIC value was increased to 12.6 μg·mL^{-1} for *C. tropicalis* and 50 μg·mL^{-1} for *C. parapsilosis* with zones of inhibitions of 10.7 ± 0.6 mm and 10 ± 1 mm, respectively. In a recent study, the MIC values of green synthesized CuO-NPs against various *Candida* species were in range of 160–300 μg·mL^{-1} [16]. Also, the MIC value of CuO-NPs against *C. albicans* was 400 μg·mL^{-1} [78]. The difference in MIC values could be attributed to different parameters such as size, shape, and surface charge [79]. Therefore, the lowest MIC value in the current study could be attributed to the small size of bacterial-synthesized CuO-NPs.

The inhibitory effects of CuO-NPs depend on several parameters such as NP concentration, contact time, temperature, size, shape, humidity, agglomeration, and surface area [80,81]. The antifungal activity of CuO-NPs can be attributed to different mechanisms such as the release of toxic ions (Cu^{2+}) due to the dissolution of CuO-NPs inside the cells. These toxic ions can cause dysfunctional proteins by reacting with –SH groups and hence destroy the essential cytoplasmic membrane proteins. Moreover, these ions can hinder or disrupt the electron transport system and hence change the membrane potential [82]. The accumulation of CuO-NPs on the cell can inhibit the conidia germination and hence suppress fungal development. Another toxic mechanism of NPs can be related to the over transcription of some genes responsible for oxidative stress that generate reactive oxygen species (ROS)

Figure 6: Activity of CuO-NPs against clinical pathogens *C. albicans*, *C. glabrata*, *C. tropicalis*, and *C. parapsilosis* at different concentrations (200, 100, 50, 25, 12.5, 6.25, and 3.13 μg·mL^{-1}).

which causes acute damage to membrane components, protein structure, nucleic acid materials, and interfere with the absorption of nutrient [83,84]. In addition, the anti-*Candida* activity of CuO-NPs could be their efficacy to alter the sterol profile in the cell wall of *Candida* species by hindering the pathway for synthesis of ergosterol [85].

3.4 *In vitro* cytotoxicity

Cancer is one of the main challenges that threaten world health that has not yet been addressed. Recently, various NPs showed high activity against different cancer cells and hence can be incorporated into cancer therapy or used as a carrier or delivery systems for drugs used in cancer treatment [16]. Before the enforcement of NPs as an antiproliferative agent against various cancer cells, the side effects and safe dose that could be used to ameliorate the harmful effects on normal cell lines should be detected. In the current study, the activity of green synthesized CuO-NPs against cancer (T47D) and normal (HFB4) cell lines were evaluated using the MTT assay method. This method is sensitive, accurate colorimetric, and target oriented to evaluate the metabolic activities of cell lines by detecting the count of viable cells after CuO-NPs treatment [86]. Data analysis showed that the toxic effect of CuO-NPs against cancer and normal cell lines was in a concentration-dependent manner that was compatible with various published investigations [29,34]. At high concentrations (1,000 $\mu g\cdot mL^{-1}$), the cell viability of cancer and normal cell lines are highly affected (cell viability = 3.7% ± 0.4% and 5.8% ± 0.3% for T47D and HFB4, respectively) (Figure 7). Similarly, the highest reduction in cell viability of colorectal cancer cells (HCT-116) was 21% at the maximum concentration used for the green synthesized CuO-NPs (35 $\mu g\cdot mL^{-1}$) [54]. Also, the CuO-NPs synthesized by *Cordia myxa* aqueous extract showed high toxic effects against breast cancer cell lines, MCF-7, and AMJ-13 decreasing the cell viability to percentages of 80.6% and 73.7%, respectively, at 100 $\mu g\cdot mL^{-1}$ after incubation times of 48 h [87]. In the current study, the cell viability was decreased by increasing the concentrations of CuO-NPs. For instance, at 125 $\mu g\cdot mL^{-1}$, the cell viability of breast cancer cells T47D was decreased by a percentage of 51% whereas the viability of normal HFB4 was decreased by a percentage of 8% (Figure 7). Andra et al. reported that the green synthesized CuO-NPs exhibit high cytotoxic efficacy against cancer cell lines as compared with those synthesized by chemical and physical approaches [88].
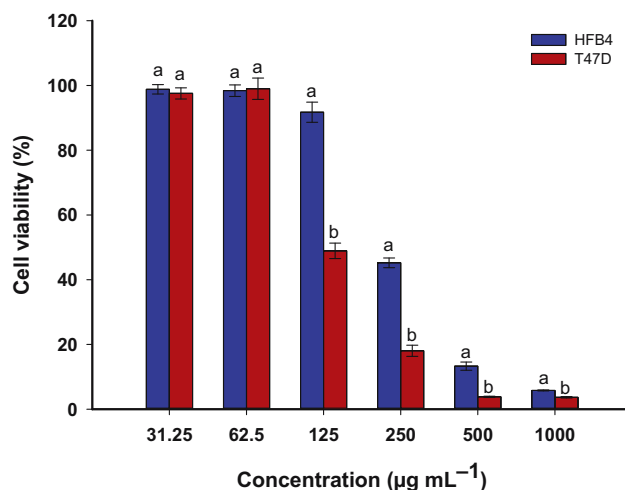
Figure 7: *In vitro* cytotoxicity of CuO-NPs against breast cancer cell lines (T47D) and normal cell lines (HFB4) detected by MTT assay method.

Herein the CuO-NP concentration required for mortality of 50% of cells (IC$_{50}$) was calculated. Data showed that the IC$_{50}$ value for normal cell lines, HFB4 was 229.9 ± 5.7 $\mu g\cdot mL^{-1}$ which represented about twice the value for cancer cell lines, T47D which was 122.3 ± 5.4 $\mu g\cdot mL^{-1}$. In a recent study, the IC$_{50}$ values of CuO-NPs fabricated by fungal strain, *Aspergillus terreus* against WI38 (normal cell lines) and Caco-2 (cancer cell lines) were 192.2 and 96.3 $\mu g\cdot mL^{-1}$, respectively [53]. Based on the obtained data, it can be concluded that the low concentration of green synthesized CuO-NPs has antiproliferative effects on cancer cell lines, while it can affect the survival, activity, and population of normal cell lines when applied at a double concentration. Hence, it is likely to exploit this target orientation to create a therapeutic window for applying CuO-NPs as a chemotherapeutic agent. In addition, the morphological changes due to treatment with various concentrations of CuO-NPs were noticed after incubation for 48 h. As shown, the cells without treatment (control) under the inverted microscope are well spread and their morphology appears as adherent epithelial cells. At high concentrations, the epithelial monolayer sheets are lost partially or completely. Also, some morphological changes such as shrinking, roundness, buoyancy, migration, and granulations appeared (Figure 8). These morphological changes disappeared gradually by decreasing the CuO-NPs concentrations.

The activity of CuO-NPs against cancer cells could be attributed to different mechanisms such as enhanced ROS production, apoptosis, antioxidant activity, autophagy, and cell cycle turned-off, which depend on the source of CuO-NPs and type of cell lines [89]. The direct
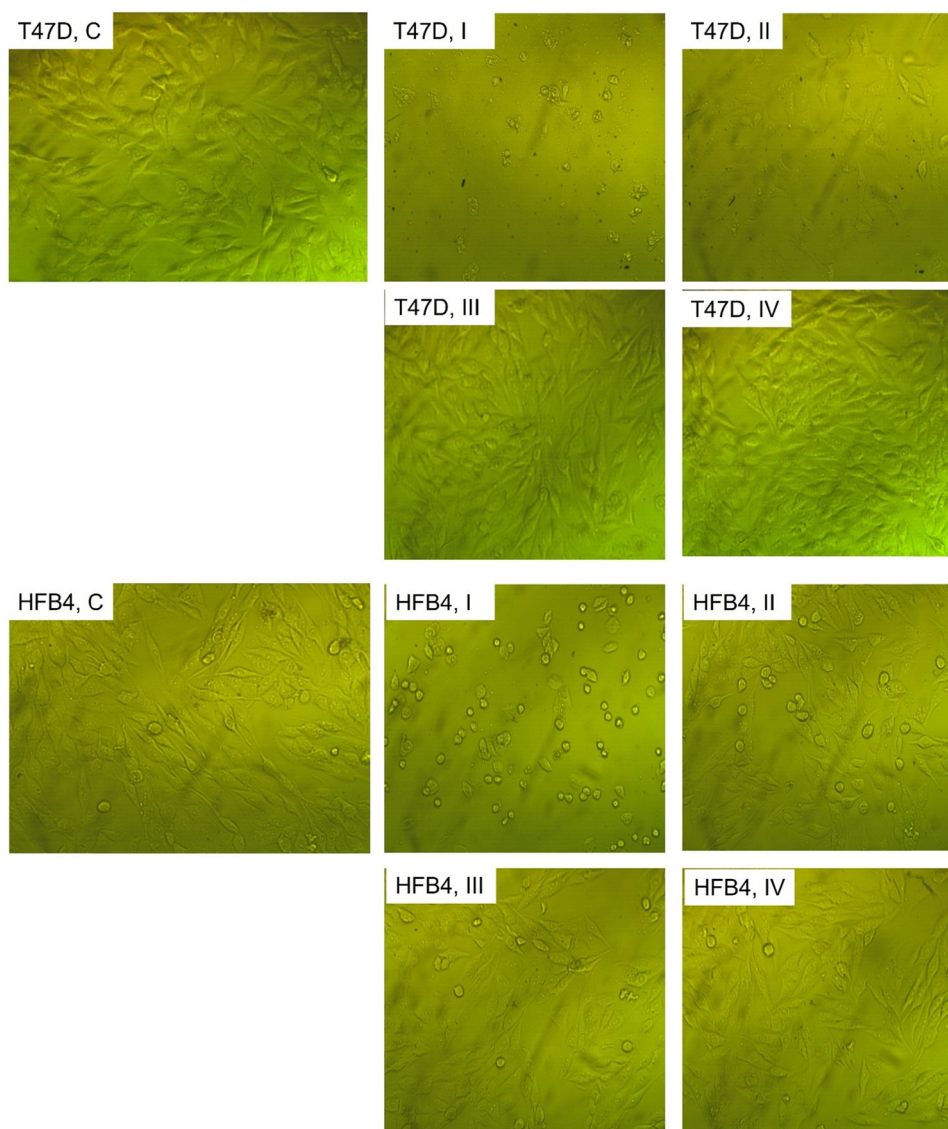
Figure 8: Morphological changes in cancer and normal cell lines due to treatment by various concentrations of CuO-NPs. T47D, C and HFB, C denote the control (without treatment); T47D, I; T47D, II; T47D, III, and T47D, IV refer to the shape of cancer cell lines T47D after treatment with 50, 25, 6.25, and 3.12 µg·mL^{-1}, respectively; HFB4, I; HFB4, II, HFB4, III, and HFB4, IV refer to the shape of normal cell lines HFB4 after treatment with 50, 25, 6.25, and 3.12 µg·mL^{-1}, respectively.

anticancer mechanism of CuO-NPs is the ROS generation or indirectly through enhanced redox reaction that ultimately leads to ROS production [65]. Upon exposure of the cell to CuO-NPs, it dissolutely forms Cu^{2+} that binds to major macromolecules inside the cells such as proteins, nucleic acid, and ribosomes leading to distortion or breakdown of these molecules, ultimately leading to cell death [89]. Also, in the cell, CuO-NPs react with mitochondria or with acidic conditions of the lysosome, leading to ROS production that is harmful to the cells [90]. ROS has damage effects on proteins, DNA, and cell membranes [91]. The most common free radicals associated with ROS toxicity are H_2O_2, $-O_2$, and $^{\bullet}OH$ [92]. Published investigations suggested that the generation of ROS in cancer cells is higher than in normal cells due to high metabolic activity in cancer cells [89], and this phenomenon is beneficial in the application of NPs in cancer therapy. Apoptosis is a mechanism for cell death controlled by a group of caspases due to DNA damage and cellular stresses [93]. This type of cell death was attained through extrinsic and intrinsic pathways. Treatment with green synthesized CuO-NPs can upregulate the expression of these pathways, leading to enhanced apoptosis [94].

3.5 Larvicidal activity

Various human and animal diseases such as filariasis, malaria, chikungunya, yellow fever, Rift Valley fever, and West Nile virus are mainly transmitted by mosquito vectors [95]. Therefore, it is important to control the spread of these vectors. The usage of chemical methods has declined due to their serious issues such as the development of resistant mosquito vectors and the toxicity of these chemical compounds to humans, animals, and plants [96]. Therefore, the development of cost-effective and low toxic substances for mosquito vector control is considered the main challenge. Due to increasing development in nano-biotechnology science and the unique properties of nanomaterials, it can be used as an alternative source for vector control. In the current study, the synthesized CuO-NPs by endophytic bacterial strain were used to control the various instar larvae of *Culex antennatus*. To the best of our knowledge, this is the first trial to utilize green synthesized CuO-NPs in the biocontrol of *C. antennatus*.

Herein the activity of bacterial-synthesized CuO-NPs to inhibit the various instar larvae of *C. antennatus* was

dependent on the concentrations. The obtained data are compatible with published investigations about the effect of various nanomaterials on the activity of mosquito vectors [97,98]. At the lowest CuO-NPs concentration (10 mg·L^{-1}), the mortality percentages were 60% ± 1.4%, 43.1% ± 1.1%, 36.2% ± 1%, and 32.1% ± 0.9% for I, II, III, and IV instar larvae, respectively (Table 1). These percentages were increased by increasing the CuO-NP concentrations to reach 64.5% ± 1.5%, 49.3% ± 1.0%, 43.1% ± 1.0%, and 35.1% ± 0.5% at 20 mg·L^{-1} and reached 86.9% ± 2.1%, 68.1% ± 1.7%, 64.4% ± 1.9%, and 53.1% ± 1.4% at the highest concentration (50 mg·L^{-1}) for the same sequence of instar larvae (Table 1). Similarly, the mortality percentages of I, II, III, and IV instar larvae of *Culex quinquefasciatus* due to treatment with 100, 250, and 500 mg·L^{-1} of CuO-NPs after 48 h were (73.3% ± 9.4%, 93.3% ± 9.4%, and 96.7% ± 4.7%), (46.7% ± 9.4%, 73.7% ± 18.9%, and 77.3% ± 4.7%), (56.0% ± 8.2%, 60.7% ± 12.5%, and 66.3% ± 4.7%), and (36.3% ± 4.3%, 43.7% ± 4.7%, and 56.7% ± 9.4%), respectively [99]. Also, the mortality percentages of III instar larvae of *Culex pipiens* were increased from 12.6% ± 0.5% to 76.8% ± 0.6% due to increase in the CuO-NPs concentration from 1 to 20 mg·L^{-1}

Table 1: Larvicidal activity of CuO-NPs against I, II, III, and IV instar larvae of *Culex antennatus*

Instar larvae	Concentrations (mg·L^{-1})	Mortality percentages (%)	LC$_{50}$ (LCL–UCL)	LC$_{90}$ (LCL–UCL)	χ^2 (*df* = 3)
I	Control	00.00 ± 0.0	2.4 (0.6–11.1)	53.6 (21.5–97.4)	7.951
	10	60.0 ± 1.4			
	20	64.5 ± 1.5			
	30	72.1 ± 0.5			
	40	82.4 ± 2.0			
	50	86.9 ± 2.1			
II	Control	00.00 ± 0.0	13.4 (4.1–25.7)	54.5 (22.5–99.4)	8.624
	10	43.1 ± 1.1			
	20	49.3 ± 1.0			
	30	55.2 ± 1.2			
	40	58.3 ± 0.5			
	50	68.1 ± 1.7			
III	Control	00.00 ± 0.0	21.9 (9.3–42.6)	62.6 (31.9–107.8)	9.361
	10	36.2 ± 0.5			
	20	43.1 ± 1.0			
	30	47.1 ± 0.4			
	40	57.1 ± 1.0			
	50	64.4 ± 1.9			
IV	Control	00.00 ± 0.0	24.4 (12.1–51.7)	65.1 (37.1–115.4)	10.529
	10	32.1 ± 0.9			
	20	35.1 ± 0.5			
	30	43.1 ± 0.7			
	40	47.2 ± 1.2			
	50	53.1 ± 1.4			

LC$_{50}$ and LC$_{90}$ – lethal CuO-NPs concentrations for 50% and 90% of larvae population, respectively; LCL and UCL – lower and upper confidence limit, respectively; χ^2 – chi-square value. Data are represented by mean value ± standard error (SE).

[23]. Based on the obtained data, the CuO-NPs synthesized by bacterial endophytes have a promising larvicidal activity at low concentrations and this could be related to the small size. Data analysis showed that the LC_{50} values (concentration for inhibiting 50% of larvae population) were 2.4, 13.4, 21.9, and 24.4 mg·L^{-1} for the first, second, third, and fourth instar larvae, respectively. Whereas the LC_{90} value (concentration for inhibiting 90% of larvae population) was 53.6, 54.5, 62.6, and 65.1 mg·L^{-1} for the same sequence of instar larvae.

The green synthesized CuO-NPs have been showing a promising insecticide activity and can be replaced by the chemical synthetic agents as reported previously [97]. In the current study, among the reasons that increase the efficacy of CuO-NPs against various instar larvae is its smaller size (2–28 nm) that facilitates its penetration through insect cuticle and hence react with macromolecules inside the cells, leading to cell death [100]. Another toxicity mechanism is the ability of CuO-NPs to dissociate into Cu^{2+} and O^{2-} inside the cell. The accumulation of toxic Cu^{2+} ions leads to the disruption the cellular equilibrium and hence more stresses were achieved causing damage to cellular components such as proteins, DNA, and amino acids leading to cell death [92]. Moreover, the high amount of O^{2-} inside the cells causes oxidative stress that leads to generating ROS ultimately leading to cell death [91].

4 Conclusion

In the current study, an environmentally friendly, cheap, simple, and rapid green approach was used to fabricate CuO-NPs to possibly integrate into various applications. Therefore, biomass filtrate of endophytic bacterial strain, *Brevibacillus brevis* PI-5 was used as a biocatalyst to reduce metal precursor and form CuO-NPs followed by capping and stabilizing as-formed final product which was characterized by UV-Vis spectroscopy, FTIR, XRD, TEM, SEM-EDX, and XPS analyses. Our study confirmed the hypothesis that suggests the biological activity of nanoparticles was size and dose dependent. Therefore, the spherical and small size of formed CuO-NPs (2–28 nm) showed a promising activity to control the growth of some important phyto-pathogenic fungi as well as inhibit the growth of various clinical *Candida* strains. Interestingly, the smaller size of synthesized CuO-NPs displayed high orientated activity toward breast cancer cell lines (T47D) at low dose compared to the activity toward normal cell lines (HFB4). Finally, bacteria-mediated CuO-NPs showed high mortality

percentages in the range from 86.9% ± 2.1% to 53.1% ± 1.4% for the instar larvae of *Culex antennatus*. The synthesized CuO-NPs need more applications against pathogenic bacteria and more cancerous cell lines to investigate their broad-spectrum activity. However, the obtained data provides a safe approach for application in the agricultural sector, biomedicine, and control of the spread of mosquito vectors to overcome the disadvantages of the usage of chemical substances.

Author contributions: Amr Fouda, Saad El-Din Hassan, and Ahmed M. Eid: conceptualization, supervision, project administration, methodology, validation, formal analysis, investigation, data curation, writing – original draft preparation, and writing – review and editing. Mohamed A. Awad, Naglaa Fathi Badr, Khalid Althumayri, and Mohammed F. Hamza: methodology, validation, formal analysis, and writing – original draft preparation.

Conflict of interest: Authors state no conflict of interest.

Data availability statement: The data used to support the findings of this study are available from the corresponding author upon request.

References

[1] Mahmoud AED, Al-Qahtani KM, Alflaij SO, Al-Qahtani SF, Alsamhan FA. Green copper oxide nanoparticles for lead, nickel, and cadmium removal from contaminated water. Sci Rep. 2021;11(1):12547.

[2] Hamza MF, Alotaibi SH, Wei Y, Mashaal NM. High-performance hydrogel based on modified chitosan for removal of heavy metal ions in borehole: A case study from the Bahariya Oasis, Egypt. Catalysts. 2022;12(7):721.

[3] Fouda A, Hassan SE-D, Abdel-Rahman MA, Farag MMS, Shehal-deen A, Mohamed AA, et al. Catalytic degradation of wastewater from the textile and tannery industries by green synthesized hematite (α-Fe$_2$O$_3$) and magnesium oxide (MgO) nanoparticles. Curr Res Biotechnol. 2021;3:29–41.

[4] Chopra H, Bibi S, Singh I, Hasan MM, Khan MS, Yousafi Q, et al. Green metallic nanoparticles: Biosynthesis to applications. Front Bioeng Biotechnol. 2022;10:874742.

[5] Shafey AME. Green synthesis of metal and metal oxide nanoparticles from plant leaf extracts and their applications: A review. Green Process Synth. 2020;9(1):304–39.

[6] Fouda A, Eid AM, Abdelkareem A, Said HA, El-Belely EF, Alkhalifah DHM, et al. Phyco-synthesized zinc oxide nanoparticles using marine macroalgae, ulva fasciata delile, characterization, antibacterial activity, photocatalysis, and tanning wastewater treatment. Catalysts. 2022;12(7):756.

[7]   Salem SS, Fouda A. Green synthesis of metallic nanoparticles and their prospective biotechnological applications: An overview. Biol Trace Elem Res. 2021;199(1):344–70.

[8]   Ghosh S, Ahmad R, Zeyaullah M, Khare SK. Microbial nano-factories: Synthesis and biomedical applications. Front Chem. 2021;9:626834.

[9]   Alsharif SM, Salem SS, Abdel-Rahman MA, Fouda A, Eid AM, El-Din Hassan S, et al. Multifunctional properties of spherical silver nanoparticles fabricated by different microbial taxa. Heliyon. 2020;6(5):e03943.

[10]   Abdo AM, Fouda A, Eid AM, Fahmy NM, Elsayed AM, Khalil AMA, et al. Green synthesis of zinc oxide nanoparticles (ZnO-NPs) by pseudomonas aeruginosa and their activity against pathogenic microbes and common house mosquito, culex pipiens. Mater (Basel, Switz). 2021;14(22):6983.

[11]   Kimber RL, Lewis EA, Parmeggiani F, Smith K, Bagshaw H, Starborg T, et al. Biosynthesis and characterization of copper nanoparticles using Shewanella oneidensis: Application for click chemistry. Small (Weinh an der Bergstrasse Ger). 2018;14(10):1703145.

[12]   Rizwana H, Alwhibi MS, Aldarsone HA, Awad MA, Soliman DA, Bhat RS. Green synthesis, characterization, and antimicrobial activity of silver nanoparticles prepared using Trigonella foenum-graecum L. leaves grown in Saudi Arabia. Green Process Synth. 2021;10(1):421–9.

[13]   Sabir S, Arshad M, Ilyas N, Naz F, Amjad MS, Malik NZ, et al. Protective role of foliar application of green-synthesized silver nanoparticles against wheat stripe rust disease caused by Puccinia striiformis. Green Process Synth. 2022;11(1):29–43.

[14]   Chakraborty N, Banerjee J, Chakraborty P, Banerjee A, Chanda S, Ray K, et al. Green synthesis of copper/copper oxide nanoparticles and their applications: A review. Green Chem Lett Rev. 2022;15(1):187–215.

[15]   Halder U, Roy RK, Biswas R, Khan D, Mazumder K, Bandopadhyay R. Synthesis of copper oxide nanoparticles using capsular polymeric substances produced by Bacillus altitudinis and investigation of its efficacy to kill pathogenic Pseudomonas aeruginosa. Chem Eng J Adv. 2022;11:100294.

[16]   Amin F, Fozia, Khattak B, Alotaibi A, Qasim M, Ahmad I, et al. Green synthesis of copper oxide nanoparticles using Aerva javanica leaf extract and their characterization and investigation of in vitro antimicrobial potential and cytotoxic activities. Evidence-Based Complementary Alternative Med. 2021;2021:5589703.

[17]   Consolo VF, Torres-Nicolini A, Alvarez VA. Mycosinthetized Ag, CuO and ZnO nanoparticles from a promising Trichoderma harzianum strain and their antifungal potential against important phytopathogens. Sci Rep. 2020;10(1):20499.

[18]   Thakar MA, Jha SS, Phasinam K, Manne R, Qureshi Y, Babu VH. X ray diffraction (XRD) analysis and evaluation of antioxidant activity of copper oxide nanoparticles synthesized from leaf extract of Cissus vitiginea. Mater Today Proc. 2022;51:319–24.

[19]   Ismail M, Gul S, Khan MI, Khan MA, Asiri AM, Khan SB. Green synthesis of zerovalent copper nanoparticles for efficient reduction of toxic azo dyes congo red and methyl orange. Green Process Synth. 2019;8(1):135–43.

[20]   Al-Musawi MMS, Al-Shmgani H, Al-Bairuty GA. Histopathological and biochemical comparative study of copper oxide nanoparticles and copper sulphate toxicity in male albino mice reproductive system. Int J Biomater. 2022;2022:4877637.

[21]   Choi L, Pryce J, Richardson M, Lutje V, Walshe D, Garner P. Guidelines for malaria vector control. World Health Organ. 2019;1–171.

[22]   Benelli G. Green synthesized nanoparticles in the fight against mosquito-borne diseases and cancer-a brief review. Enzyme Microb Technol. 2016;95:58–68.

[23]   Mostafa WA, Abdel-Raoof AM, Attala K, Elgazzar E. Enhancement the larvicidal activity of nanostructure copper oxide against Culex pipiens mosquito by yttrium replacement based on crystallite size reduction and topographic surface nature. Mater Res Exp. 2021;8(11):115006.

[24]   Fouda A, Eid AM, Elsaied A, El-Belely EF, Barghoth MG, Azab E, et al. Plant growth-promoting endophytic bacterial community inhabiting the leaves of pulicaria incisa (Lam.) DC inherent to arid regions. Plants (Basel, Switz). 2021;10(1):76.

[25]   Mahgoub HAM, Fouda A, Eid AM, Ewais EE-D, Hassan SE-D. Biotechnological application of plant growth-promoting endophytic bacteria isolated from halophytic plants to ameliorate salinity tolerance of Vicia faba L. Plant Biotechnol Rep. 2021;15(6):819–43.

[26]   Vos P, Garrity G, Jones D, Krieg NR, Ludwig W, Rainey FA, et al. Bergey's manual of systematic bacteriology. 3, The Firmicutes. Springer: New York, NY; 2011.

[27]   Fouda A, Salem SS, Wassel AR, Hamza MF, Shaheen TI. Optimization of green biosynthesized visible light active CuO/ZnO nano-photocatalysts for the degradation of organic methylene blue dye. Heliyon. 2020;6(9):e04896.

[28]   Hamza MF, Lu S, Salih KAM, Mira H, Dhmees AS, Fujita T, et al. As(V) sorption from aqueous solutions using quaternized algal/polyethyleneimine composite beads. Sci Total Environ. 2020;719:137396.

[29]   Zhao H, Maruthupandy M, Al-mekhlafi FA, Chackaravarthi G, Ramachandran G, Chelliah CK. Biological synthesis of copper oxide nanoparticles using marine endophytic actinomycetes and evaluation of biofilm producing bacteria and A549 lung cancer cells. J King Saud Univ - Sci. 2022;34(3):101866.

[30]   Hamza MF, Wei Y, Althumayri K, Fouda A, Hamad NA. Synthesis and Characterization of Functionalized Chitosan Nanoparticles with Pyrimidine Derivative for Enhancing Ion Sorption and Application for Removal of Contaminants. Mater (Basel, Switz). 2022;15(13):4676.

[31]   Ghaffar N, Javad S, Farrukh MA, Shah AA, Gatasheh MK, Al-Munqedhi BMA, et al. Metal nanoparticles assisted revival of Streptomycin against MDRS Staphylococcus aureus. PLoS One. 2022;17(3):e0264588.

[32]   Wei Y, Salih KAM, Lu S, Hamza MF, Fujita T, Vincent T, et al. Amidoxime Functionalization of Algal/Polyethyleneimine Beads for the Sorption of Sr(ɪɪ) from Aqueous Solutions. Molecules (Basel, Switz). 2019;24(21):3893.

[33]   Fouda A, Hassan SE-D, Eid AM, Abdel-Rahman MA, Hamza MF. Light enhanced the antimicrobial, anticancer, and catalytic activities of selenium nanoparticles fabricated by endophytic fungal strain, Penicillium crustosum EP-1. Sci Rep. 2022;12(1):11834.

[34] Fouda A, Eid AM, Abdel-Rahman MA, El-Belely EF, Awad MA, Hassan SE, et al. Enhanced antimicrobial, cytotoxicity, larvicidal, and repellence activities of brown algae, Cystoseira crinita-mediated green synthesis of magnesium oxide nanoparticles. Front Bioeng Biotechnol. 2022;10:849921.

[35] World Health Organization. Informal consultation on the evaluation on the testing of insecticides. Geneva, Switzerland: WHO; 2020. p. 69. CTD/WHO PES/IC/96.1.

[36] Abbott WS. A method of computing the effectiveness of an insecticide. J Economic Entomol. 1925;18(2):265–7.

[37] Fouda A, Hassan SE, Abdo AM, El-Gamal MS. Antimicrobial, antioxidant and larvicidal activities of spherical silver nanoparticles synthesized by endophytic Streptomyces spp. Biol Trace Elem Res. 2020;195(2):707–24.

[38] Syed B, Prasad MN, Satish S. Synthesis and characterization of silver nanobactericides produced by Aneurinibacillus migulanus 141, a novel endophyte inhabiting Mimosa pudica L. Arab J Chem. 2019;12(8):3743–52.

[39] Eid AM, Fouda A, Abdel-Rahman MA, Salem SS, Elsaied A, Oelmüller R, et al. Harnessing bacterial endophytes for promotion of plant growth and biotechnological applications: An overview. Plants. 2021;10(5):935.

[40] Filippi A, Mattiello A, Musetti R, Petrussa E, Braidot E, Marchiol L. In *Green synthesis of Ag nanoparticles using plant metabolites*. AIP Conference Proceedings. AIP Publishing LLC; 2017. p. 020004.

[41] Shantkriti S, Rani P. Biological synthesis of copper nanoparticles using Pseudomonas fluorescens. Int J Curr Microbiol App Sci. 2014;3(9):374–83.

[42] Hassan SE, Fouda A, Radwan AA, Salem SS, Barghoth MG, Awad MA, et al. Endophytic actinomycetes Streptomyces spp mediated biosynthesis of copper oxide nanoparticles as a promising tool for biotechnological applications. J Biol Inorg Chem JBIC a Publ Soc Biol Inorg Chem. 2019;24(3):377–93.

[43] Jayakumarai G, Gokulpriya C, Sudhapriya R, Sharmila G, Muthukumaran C. Phytofabrication and characterization of monodisperse copper oxide nanoparticles using Albizia lebbeck leaf extract. Appl Nanosci. 2015;5(8):1017–21.

[44] Karthik C, Suresh S, Sneha Mirulalini G, Kavitha S. A FTIR approach of green synthesized silver nanoparticles by Ocimum sanctum and Ocimum gratissimum on mung bean seeds. Inorg Nano-Metal Chem. 2020;50(8):606–12.

[45] Lashin I, Fouda A, Gobouri AA, Azab E, Mohammedsaleh ZM, Makharita RR. Antimicrobial and *in vitro* cytotoxic efficacy of biogenic silver nanoparticles (Ag-NPs) fabricated by callus extract of Solanum incanum L. Biomolecules. 2021;11(3):341.

[46] Hamza MF, Fouda A, Wei Y, El Aassy IE, Alotaibi SH, Guibal E, et al. Functionalized biobased composite for metal decontamination – Insight on uranium and application to water samples collected from wells in mining areas (Sinai, Egypt). Chem Eng J. 2022;431:133967.

[47] Badawy AA, Abdelfattah NAH, Salem SS, Awad MF, Fouda A. Efficacy Assessment of Biosynthesized Copper Oxide Nanoparticles (CuO-NPs) on Stored Grain Insects and Their Impacts on Morphological and Physiological Traits of Wheat (Triticum aestivum L.) Plant. Biology. 2021;10(3):233.

[48] Saha N, Trivedi P, Dutta Gupta S. Surface plasmon resonance (SPR) based optimization of biosynthesis of silver nanoparticles from rhizome extract of Curculigo orchioides

gaertn and its antioxidant potential. J Clust Sci. 2016;27(6):1893–912.

[49] Hamza MF, Hamad DM, Hamad NA, Abdel-Rahman AAH, Fouda A, Wei Y, et al. Functionalization of magnetic chitosan microparticles for high-performance removal of chromate from aqueous solutions and tannery effluent. Chem Eng J. 2022;428:131775.

[50] Coates J. Interpretation of infrared spectra, a practical approach, in encyclopedia of analytical chemistry, applications, theory and instrumentation. Infrared spectroscopy in analysis of polymer crystallinity. Hoboken, NJ, USA: John Wiley & Sons; 2000.

[51] Sarkar J, Chakraborty N, Chatterjee A, Bhattacharjee A, Dasgupta D, Acharya K. Green Synthesized Copper Oxide Nanoparticles Ameliorate Defence and Antioxidant Enzymes in Lens culinaris. Nanomater (Basel, Switz). 2020;10(2):312.

[52] Rani Verma P, Khan F. Green approach for biofabrication of CuO nanoparticles from Prunus amygdalus pericarp extract and characterization. Inorg Nano-Metal Chem. 2019;49(3):69–74.

[53] Shaheen TI, Fouda A, Salem SS. Integration of cotton fabrics with biosynthesized CuO nanoparticles for bactericidal activity in the terms of their cytotoxicity assessment. Ind Eng Chem Res. 2021;60(4):1553–63.

[54] Tabrez S, Khan AU, Mirza AA, Suhail M, Jabir NR, Zughaibi TA, et al. Biosynthesis of copper oxide nanoparticles and its therapeutic efficacy against colon cancer. Nanotechnol Rev. 2022;11(1):1322–31.

[55] Bukhari SI, Hamed MM, Al-Agamy MH, Gazwi HSS, Radwan HH, Youssif AM. Biosynthesis of copper oxide nanoparticles using streptomyces MHM38 and its biological applications. J Nanomater. 2021;2021:6693302.

[56] Azam A, Ahmed AS, Oves M, Khan MS, Memic A. Size-dependent antimicrobial properties of CuO nanoparticles against Gram-positive and -negative bacterial strains. Int J Nanomed. 2012;7:3527–35.

[57] Mancuso L, Cao G. Acute toxicity test of CuO nanoparticles using human mesenchymal stem cells. Toxicol Mechan Methods. 2014;24(7):449–54.

[58] Sharma S, Kumar K, Thakur N, Chauhan S, Chauhan MS. The effect of shape and size of ZnO nanoparticles on their antimicrobial and photocatalytic activities: A green approach. Bull Mater Sci. 2019;43(1):20.

[59] Mohamed AA, Fouda A, Abdel-Rahman MA, Hassan SE-D, El-Gamal MS, Salem SS, et al. Fungal strain impacts the shape, bioactivity and multifunctional properties of green synthesized zinc oxide nanoparticles. Biocatal Agric Biotechnol. 2019;19:101103.

[60] Scimeca M, Bischetti S, Lamsira HK, Bonfiglio R, Bonanno E. Energy dispersive X-ray (EDX) microanalysis: A powerful tool in biomedical research and diagnosis. Eur J Histochem. 2018;62(1):2841.

[61] Qamar H, Rehman S, Chauhan DK, Tiwari AK, Upmanyu V. Green synthesis, characterization and antimicrobial activity of copper oxide nanomaterial derived from momordica charantia. Int J Nanomed. 2020;15:2541–53.

[62] Fouda A, Hassan SE-D, Saied E, Hamza MF. Photocatalytic degradation of real textile and tannery effluent using biosynthesized magnesium oxide nanoparticles (MgO-NPs),

heavy metal adsorption, phytotoxicity, and antimicrobial activity. J Environ Chem Eng. 2021;9(4):105346.

[63] Alhalili Z. Green synthesis of copper oxide nanoparticles CuO NPs from Eucalyptus Globoulus leaf extract: Adsorption and design of experiments. Arab J Chem. 2022;15(5):103739.

[64] Ahamed M, Alhadlaq HA, Khan MAM, Karuppiah P, Al-Dhabi NA. Synthesis, characterization, and antimicrobial activity of copper oxide nanoparticles. J Nanomaterials. 2014;2014:637858.

[65] Naz S, Gul A, Zia M. Toxicity of copper oxide nanoparticles: A review study. IET Nanobiotechnol. 2020;14(1):1–13.

[66] Jurado-López B, Vieira RS, Rabelo RB, Beppu MM, Casado J, Rodríguez-Castellón E. Formation of complexes between functionalized chitosan membranes and copper: A study by angle resolved XPS. Mater Chem Phys. 2017;185:152–61.

[67] Yang K, Zhong L, Guan R, Xiao M, Han D, Wang S, et al. Carbon felt interlayer derived from rice paper and its synergistic encapsulation of polysulfides for lithium-sulfur batteries. Appl Surf Sci. 2018;441:914–22.

[68] Lu S, Chen L, Hamza MF, He C, Wang X, Wei Y, et al. Amidoxime functionalization of a poly(acrylonitrile)/silica composite for the sorption of Ga(III) – Application to the treatment of Bayer liquor. Chem Eng J. 2019;368:459–73.

[69] Peng Y, Li SJ, Yan J, Tang Y, Cheng JP, Gao AJ, et al. Research progress on phytopathogenic fungi and their role as biocontrol agents. Front Microbiol. 2021;12:670135.

[70] Bernardo-Mazariegos E, Valdez-Salas B, González-Mendoza D, Abdelmoteleb A, Tzintzun Camacho O, Ceceña Duran C, et al. Silver nanoparticles from Justicia spicigera and their antimicrobial potentialities in the biocontrol of foodborne bacteria and phytopathogenic fungi. Rev Argentina de Microbiol. 2019;51(2):103–9.

[71] Hassan SELD, Salem SS, Fouda A, Awad MA, El-Gamal MS, Abdo AM. New approach for antimicrobial activity and biocontrol of various pathogens by biosynthesized copper nanoparticles using endophytic actinomycetes. J Radiat Res Appl Sci. 2018;11(3):262–70.

[72] Bhavyasree PG, Xavier TS. Green synthesis of Copper Oxide/ Carbon nanocomposites using the leaf extract of Adhatoda vasica Nees, their characterization and antimicrobial activity. Heliyon. 2020;6(2):e03323.

[73] Gajdács M, Dóczi I, Ábrók M, Lázár A, Burián K. Epidemiology of candiduria and Candida urinary tract infections in inpatients and outpatients: Results from a 10-year retrospective survey. Cent Eur J Urol. 2019;72(2):209–14.

[74] Rabiee N, Bagherzadeh M, Kiani M, Ghadiri AM, Etessamifar F, Jaberizadeh AH, et al. Biosynthesis of copper oxide nanoparticles with potential biomedical applications. Int J Nanomed. 2020;15:3983–99.

[75] John MS, Nagoth JA, Zannotti M, Giovannetti R, Mancini A, Ramasamy KP, et al. Biogenic synthesis of copper nanoparticles using bacterial strains isolated from an antarctic consortium associated to a psychrophilic marine ciliate: characterization and potential application as antimicrobial agents. Mar Drugs. 2021;19(5):263.

[76] Hawar SN, Al-Shmgani HS, Al-Kubaisi ZA, Sulaiman GM, Dewir YH, Rikisahedew JJ. Green synthesis of silver nanoparticles from alhagi graecorum leaf extract and evaluation of their cytotoxicity and antifungal activity. J Nanomater. 2022;2022:1058119.

[77] Kowalska-Krochmal B, Dudek-Wicher R. The minimum inhibitory concentration of antibiotics: Methods, interpretation, clinical relevance. Pathogens. 2021;10(2):165.

[78] Karimiyan A, Najafzadeh H, Ghorbanpour M, Hekmati-Moghaddam SH. Antifungal effect of magnesium oxide, zinc oxide, silicon oxide and copper oxide nanoparticles against Candida albicans. Zahedan J Res Med Sci. 2015;17(10):2179.

[79] Khan MF, Hameedullah M, Ansari AH, Ahmad E, Lohani M, Khan RH, et al. Flower-shaped ZnO nanoparticles synthesized by a novel approach at near-room temperatures with antibacterial and antifungal properties. Int J Nanomed. 2014;9:853.

[80] Arendsen LP, Thakar R, Sultan AH. The use of copper as an antimicrobial agent in health care, including obstetrics and gynecology. Clin Microbiol Rev. 2019;32(4):e00125–18.

[81] Fouda A, Awad MA, Al-Faifi ZE, Gad ME, Al-Khalaf AA, Yahya R, et al. Aspergillus flavus-mediated green synthesis of silver nanoparticles and evaluation of their antibacterial, anti-candida, acaricides, and photocatalytic activities. Catalysts. 2022;12(5):462.

[82] Cruz-Luna AR, Cruz-Martínez H, Vásquez-López A, Medina DI. Metal nanoparticles as novel antifungal agents for sustainable agriculture: Current advances and future directions. J Fungi. 2021;7(12):1033.

[83] Huerta-García E, Pérez-Arizti JA, Márquez-Ramírez SG, Delgado-Buenrostro NL, Chirino YI, Iglesias GG, et al. Titanium dioxide nanoparticles induce strong oxidative stress and mitochondrial damage in glial cells. Free Radic Biol Med. 2014;73:84–94.

[84] Fouda A, Awad MA, Eid AM, Saied E, Barghoth MG, Hamza MF, et al. An eco-friendly approach to the control of pathogenic microbes and anopheles stephensi malarial vector using magnesium oxide nanoparticles (Mg-NPs) fabricated by Penicillium chrysogenum. Int J Mol Sci. 2021;22(10):5096.

[85] Abd-Elaziz AM, Aly HM, Saleh NM, Fouad SA, Ismail AA, Fouda A. Synthesis and characterization of the novel pyrimidine's derivatives, as a promising tool for antimicrobial agent and in vitro cytotoxicity. J Iran Chem Soc. 2022;19(6):2279–96.

[86] Ghasemi M, Turnbull T, Sebastian S, Kempson I. The MTT Assay: Utility, limitations, pitfalls, and interpretation in bulk and single-cell analysis. Int J Mol Sci. 2021;22(23):12827.

[87] Ali Thamer N, Tareq Barakat N. Cytotoxic activity of green synthesis copper oxide nanoparticles using cordia myxa L. aqueous extract on some breast cancer cell lines. J Phys Conf Ser. 2019;1294(6):062104.

[88] Andra S, Balu SK, Jeevanandham J, Muthalagu M, Vidyavathy M, Chan YS, et al. Phytosynthesized metal oxide nanoparticles for pharmaceutical applications. Naunyn Schmiedebergs Arch Pharmacol. 2019;392(7):755–71.

[89] Letchumanan D, Sok SPM, Ibrahim S, Nagoor NH, Arshad NM. Plant-Based Biosynthesis of Copper/Copper Oxide Nanoparticles: An Update on Their Applications in Biomedicine, Mechanisms, and Toxicity. Biomolecules. 2021;11(4):564.

[90] Xia T, Kovochich M, Liong M, Mädler L, Gilbert B, Shi H, et al. Comparison of the mechanism of toxicity of zinc oxide and cerium oxide nanoparticles based on dissolution and oxidative stress properties. ACS Nano. 2008;2(10):2121–34.

[91] Privalova LI, Katsnelson BA, Loginova NV, Gurvich VB, Shur VY, Valamina IE, et al. Subchronic toxicity of copper oxide nanoparticles and its attenuation with the help of a combination of bioprotectors. Int J Mol Sci. 2014;15(7):12379–406.

[92] Hassan SE, Fouda A, Saied E, Farag MMS, Eid AM, Barghoth MG, et al. Rhizopus oryzae-mediated green synthesis of magnesium oxide nanoparticles (MgO-NPs): A promising tool for antimicrobial, mosquitocidal action, and tanning effluent treatment. J Fungi. 2021;7(5):372.

[93] Pfeffer CM, Singh ATK. Apoptosis: A target for anticancer therapy. Int J Mol Sci. 2018;19(2):448.

[94] Ali K, Saquib Q, Ahmed B, Siddiqui MA, Ahmad J, Al-Shaeri M, et al. Bio-functionalized CuO nanoparticles induced apoptotic activities in human breast carcinoma cells and toxicity against Aspergillus flavus: An *in vitro* approach. Process Biochem. 2020;91:387–97.

[95] Lee H, Halverson S, Ezinwa N. Mosquito-borne diseases. Prim Care ClOffice Pract. 2018;45(3):393–407.

[96] Liu N. Insecticide resistance in mosquitoes: Impact, mechanisms, and research directions. Annu Rev Entomol. 2015;60:537–59.

[97] Muthamil Selvan S, Vijai Anand K, Govindaraju K, Tamilselvan S, Kumar VG, Subramanian KS, et al. Green synthesis of copper oxide nanoparticles and mosquito larvicidal activity against dengue, zika and chikungunya causing vector Aedes aegypti. IET Nanobiotechnol. 2018;12(8):1042–6.

[98] Awad MA, Eid AM, Elsheikh TMY, Al-Faifi ZE, Saad N, Sultan MH, et al. Mycosynthesis, characterization, and mosquitocidal activity of silver nanoparticles fabricated by Aspergillus niger strain. J Fungi (Basel, Switz). 2022;8(4):396.

[99] Chakrabarti A, Patra P. Relative larvicidal property of common oxide nanostructures against Culex quinquefasciatus. IET Nanobiotechnol. 2020;14(5):389–95.

[100] Suresh U, Murugan K, Panneerselvam C, Rajaganesh R, Roni M, Aziz AT, et al. Suaeda maritima-based herbal coils and green nanoparticles as potential biopesticides against the dengue vector Aedes aegypti and the tobacco cutworm Spodoptera litura. Physiol Mol Plant Pathol. 2018;101:225–35.